Appl. Phys. A 00, 1–7 (2004)
DOI: 10.1007/s00339-003-2459-z

Applied Physics A
Materials Science & Processing

R. SAITO[1,✉]
A. GRÜNEIS[1]
G.G. SAMSONIDZE[2]
G. DRESSELHAUS[2]
M.S. DRESSELHAUS[2]
A. JORIO[3]
L.G. CANÇADO[3]
M.A. PIMENTA[3]
A.G. SOUZA FILHO[4]

Optical absorption of graphite and single-wall carbon nanotubes

[1] Department of Physics, Tohoku University and CREST JST, Aoba Sendai 980-8578, Japan
[2] Massachusetts Institute of Technology, Cambridge, MA 02139-4307, USA
[3] Departamento de Física, Universidade Federal de Minas Gerais, Caixa Postal 702, Belo Horizonte, MG, 30123-970, Brazil
[4] Departamento de Física, Universidade Federal do Ceará, Fortaleza, CE, 60455-760, Brazil

Received: 31 July 2003/Accepted: 22 October 2003
Published online: ■ ■ 2004 • © Springer-Verlag 2004

ABSTRACT A review of the electronic dipole transitions in graphite and single-wall carbon nanotubes is presented. Because of its singular electronic structure, the optical absorption matrix element as a function of wave vector has a node in the two-dimensional Brillouin zone of graphite, which depends linearly on the optical polarization direction. In the case of the single-wall carbon nanotubes, the dipole selection rule and the van Hove singularity in the joint density of states will give a characteristic behavior, which is observed by luminescence and Raman spectroscopy.

PACS 78.30.Na; 78.20.Bh; 78.66.Tr; 63.22.+m; 36.20.Kd; 36.20.Ng

1 Introduction

A single-wall carbon nanotube (SWNT) has a nanometer-sized length along the nanotube diameter and a length of several microns in the nanotube-axis direction [1, 2]. Since the wavelength of light lies in between these two characteristic lengths, the optical behavior of SWNTs is unique in the sense that the behavior exhibits both a molecular nature and a solid-state nature. For the molecular nature of SWNTs, the optical absorption spectra are rich and sharp because of the quantization of wave vectors k along the circumferential direction of the one-dimensional (1D) system to form 1D electronic energy bands, which give sharp van Hove singularities (vHSs) in the joint density of states (JDOS), just like a molecular level [2, 3]. For the solid-state nature of SWNTs, the wave vector k is continuous in the direction of the nanotube axis, and scattering or relaxation behavior occurs by phonons or conduction electrons. The co-existence of the two concepts in a SWNT gives rise to a unique behavior in the optical properties of SWNTs.

Furthermore, the electronic structure of the unfolded SWNTs, that is two-dimensional (2D) graphite (or graphene), is unique in its own right. The conduction and the valence bands, which consist of π-electron states, touch each other at the corners of the hexagonal Brillouin zone (BZ), known as the K and K' points (see Fig. 1) [2]. The reason why the energy bands are degenerate at the BZ boundary is that there are two equivalent carbon atoms denoted by A and B in the unit cell. Because of the high symmetry between the A and B atoms, no energy gap is opened at the K and K' points. However, when the A and B atoms are not the same (for example, in the case of boron nitride, BN), an energy gap is indeed opened at the zone boundary. In fact, BN becomes a wide-band-gap semiconductor. In the case of diamond which has sp^3 bonding, on the other hand, there are two equivalent carbon atoms in the unit cell, and thus we can see an energy-band degeneracy at the zone boundary of the three-dimensional (3D) BZ. However, this energy at the BZ boundary does not correspond to the Fermi energy, and thus diamond becomes a wide-gap semiconductor. Graphite is a unique material in nature, exhibiting energy bands at the Fermi level that are doubly degenerate, without considering electron spin. Another unique aspect of 2D graphite is the fact that the Fermi wave vector exists at the zone boundary of the 2D BZ. Furthermore, the energy-dispersion relations for both the valence and conduction bands are linear around the Fermi energy. This situation is analogous to that for a massless neutrino particle. In fact, the effective-mass equation for 2D graphite has the same structure as Weyl's equation of relativistic quantum physics [4, 5]. This special electronic structure of 2D graphite gives rise to the unique and exotic physical properties of single-wall carbon nanotubes [1, 2], such as: (1) being ei-

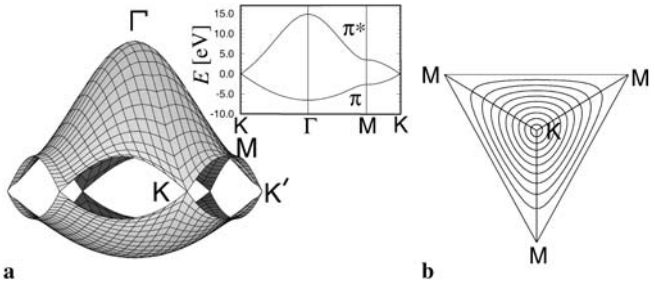

FIGURE 1 **a** The energy-dispersion relations for the π and π^* bands in 2D graphite (or graphene) are shown in the 2D Brillouin zone. The *inset* shows the energy dispersion along the high-symmetry directions of the 2D BZ. **b** The contour plot of the 2D energy bands of graphite. The equi-energy contours are circles near K and near the center of the Brillouin zone, but near the zone boundary the contours are straight lines which connect nearest M points CE[a]

✉ Fax: ■, E-mail: rsaito@flex.phys.tohoku.ac.jp

CE[a] Figure 1a is not referred to in the text.

Editor's or typesetter's annotations (will be removed before the final TEX run)

ther metallic or semiconducting depending on diameter and chirality [6, 7], (2) absence of back scattering in their transport properties [8], (3) inter-valley double-resonance Raman scattering [9–11], and (4) nodes in the optical absorption as a function of k [12].

Optical measurements provide a useful and quick tool for characterizing a single SWNT on a Si/SiO_2 substrate [13] or in an aqueous SDS CE:b suspension [15, 16], since there is no need to make contacts to the sample. By focusing a small spot of laser light, we can get a spatial resolution of up to 1 μm or less [13, 17]. By changing the laser energy, we can get a high energy resolution of 3 meV in the measurement of the energy of a vHS by resonance Raman spectroscopy [18].

In this article, we review the standard theory of optical dipole transitions in 2D graphite and in SWNTs [12] and the dipole selection rules for each of these cases [5, 19, 20]. Then we compare some experimental results of luminescence [15, 16, 21, 22] and resonance Raman spectroscopy [13, 23, 24] for which the electron–photon interaction is essential.

2 Optical dipole transitions in graphite

First we consider the optical dipole transition of 2D graphite [12, 20]. For a laser energy less than 3 eV, the optical transition occurs between bonding π and π^* energy bands. The dipole selection rule tells us that an optical transition for the 2p orbitals of an atom is not allowed. However, the transition from a 2p orbital of one atom to that of a neighboring atom is allowed, which gives the π–π^* transition in graphite and in carbon nanotubes.

Time-dependent perturbation theory for an electro-magnetic wave field provides us with the matrix element for the dipole absorption or emission between an initial state (Ψ_i) and a final state $\left(\Psi_f\right)$, which is given by [12, 20]

$$M_{i\to f}^{j=\mathrm{a,e}} = \mathrm{i}\frac{e\hbar}{m\omega}\sqrt{\frac{I}{\varepsilon c}}\,\mathrm{e}^{\mathrm{i}(\omega_f-\omega_i\mp\omega_j)t}\,\boldsymbol{P}\langle\Psi_f|\nabla|\Psi_i\rangle\,, \tag{1}$$

where I, ω, and $\boldsymbol{P}$ are intensity, frequency, and polarization vectors of the optical electric field, respectively, and the sign '$\mp$' in (1) corresponds to the light absorption ($j=\mathrm{a}$) or emission ($j=\mathrm{e}$).

The matrix element is given by an inner product of the polarization vector $\boldsymbol{P}$ and the dipole vector $\boldsymbol{D}$ defined by

$$\boldsymbol{D} \equiv \langle\Psi_f|\nabla|\Psi_i\rangle\,. \tag{2}$$

In order for the dipole transitions to occur, we need to have a finite length of the dipole vector perpendicular to the wave-propagation direction or parallel to the polarization vector.

In the case of a graphene layer, the wavefunction Ψ_l ($l=i,\ f$) can be written as a sum of two Bloch functions Φ_s ($s=\mathrm{A,\,B}$) for the A and B atoms,

$$\Psi_l\left(\boldsymbol{k}_l,\boldsymbol{r}\right) = \sum_{s=\mathrm{A,B}} C_s^l\left(\boldsymbol{k}_l\right)\Phi_s\left(\boldsymbol{k}_l,\boldsymbol{r}\right)\,, \tag{3}$$

where the coefficient $C_s^l\left(\boldsymbol{k}_l\right)$ is obtained by solving this 2×2 Hamiltonian matrix [2]. Each Bloch function Φ_s ($s=\mathrm{A,\,B}$) is further expressed by a linear combination of atomic $2\mathrm{p}_z$ orbitals $\varphi\left(\boldsymbol{r}-\boldsymbol{R}_j\right)$ ($j=1,\ldots,N$). In the tight-binding approximation, the summation is taken over the solid, and N is the number of unit cells:

$$\Phi_s\left(\boldsymbol{k}_l,\boldsymbol{r}\right) = \frac{1}{\sqrt{N}}\sum_{j=1}^{N}\mathrm{e}^{\mathrm{i}\boldsymbol{k}_l\boldsymbol{R}_j}\varphi\left(\boldsymbol{r}-\boldsymbol{R}_j\right)\,. \tag{4}$$

Substituting (4) into (2), the dipole matrix vector is expressed by a linear combination of atomic dipole matrix vectors:

$$\boldsymbol{D}_{\mathrm{a}}\left(\boldsymbol{R}_1,\boldsymbol{R}_2\right) \equiv \langle\varphi\left(\boldsymbol{r}-\boldsymbol{R}_1\right)|\nabla|\,\varphi\left(\boldsymbol{r}-\boldsymbol{R}_2\right)\rangle\,, \tag{5}$$

where $\boldsymbol{D}_{\mathrm{a}}\left(\boldsymbol{R}_1,\boldsymbol{R}_2\right)$ is the atomic dipole vector between two orbitals at $\boldsymbol{R}_1$ and $\boldsymbol{R}_2$. The atomic dipole vector within the same atom, ($\boldsymbol{R}_1=\boldsymbol{R}_2$), becomes zero, that is, $\boldsymbol{D}_{\mathrm{a}}\left(\boldsymbol{R}_1,\boldsymbol{R}_1\right)=0$.

When we put a graphene layer on the xy plane, then the z component of any atomic dipole vector between two atoms at $\boldsymbol{R}_1$ and $\boldsymbol{R}_2$ for the derivative on z becomes zero,

$$\boldsymbol{D}_{\mathrm{a}}^{z}\left(\boldsymbol{R}_1,\boldsymbol{R}_2\right) = \left\langle\varphi\left(\boldsymbol{r}-\boldsymbol{R}_{j1}\right)\left|\frac{\partial}{\partial z}\right|\varphi\left(\boldsymbol{r}-\boldsymbol{R}_{j2}\right)\right\rangle = 0\,, \tag{6}$$

because the integrand is an odd function of z. Thus the atomic dipole vector for each carbon atom has a direction parallel to the graphitic plane, $\boldsymbol{D}=\left(d_x,d_y,0\right)$. Thus 2D graphite strongly absorbs light that is incident perpendicular to the graphite plane, $\boldsymbol{P}=\left(p_x,p_y,0\right)$. Hereafter, we concentrate only on the in-plane polarization optical resonance. It should be mentioned that we need to consider out-of-plane polarization in the case of small-diameter SWNTs since the curvature effect can not be neglected.

The matrix element for the derivative on x (or y) has a non-vanishing value if the relative position $\boldsymbol{R}_{j1}-\boldsymbol{R}_{j2}$ has an x (or y) component. When we consider the matrix elements only for the three nearest-neighbor atoms, we get the following formulation,

$$\begin{aligned}&\langle\Psi_c(\boldsymbol{k})|\nabla|\Psi_v(\boldsymbol{k})\rangle\\ &= \frac{2\sqrt{3}M}{a}\,\mathrm{Re}\left[C_{\mathrm{A}}^{c*}(\boldsymbol{k})C_{\mathrm{B}}^{v}(\boldsymbol{k})\sum_{i=1}^{3}\mathrm{e}^{\mathrm{i}\boldsymbol{k}\cdot\boldsymbol{b}_i}\boldsymbol{b}_i\right]\,,\end{aligned} \tag{7}$$

where $a=2.46$ Å is the lattice constant of graphite, Re[...] is the real part of [...], and $\boldsymbol{b}_i$ ($i=1,3$) denotes the nearest-neighbor carbon-atom vectors from A to B sites. Here $\boldsymbol{b}_1=(-a_{\mathrm{C\text{–}C}},0,0)$ has a bond length $a_{\mathrm{C\text{–}C}}=a/\sqrt{3}=1.42$ Å, while $\boldsymbol{b}_2$ and $\boldsymbol{b}_3$ are given by rotating $\boldsymbol{b}_1$ by $2\pi/3$ and $4\pi/3$, respectively. It is noted that we used for (7) the following relation: $C_{\mathrm{A}}^{v*}C_{\mathrm{B}}^{c}=-\left(C_{\mathrm{B}}^{v*}C_{\mathrm{A}}^{c}\right)^*$, which can be directly shown by using the analytic form of C_j^i. Also, M in (7) is the optical matrix element for the two nearest-neighbor atoms separated by $\boldsymbol{b}_1$:

$$M = \left\langle\varphi\left(\boldsymbol{R}+\boldsymbol{b}_1\right)\left|\frac{\partial}{\partial x}\right|\varphi(\boldsymbol{R})\right\rangle\,. \tag{8}$$

For light with energy smaller than 3 eV, the optical absorption occurs around the K and K' points (hexagonal corners) of the 2D BZ (see Fig. 1). The coordinates of the two inequivalent K points in the 2D BZ are $K=(0,-4\pi/3a)$ and $K'=(0,4\pi/3a)$, respectively. In this case, (7) is expanded as a Taylor series in $\boldsymbol{k}$ around the K (or K') point. Hereafter, all

CE:b Please define SDS.

Editor's or typesetter's annotations (will be removed before the final TEX run)

coordinates of $\boldsymbol{k}$ in the Taylor expansions are measured from the K point. The coefficients of the wavefunction can be expressed as a linear function of $\boldsymbol{k}$ [8, 25] and they are expanded around the K (or K') point as

$$C_{\mathrm{A}}^{c}(\boldsymbol{k}) = \frac{1}{\sqrt{2}}\,, \quad C_{\mathrm{B}}^{c}(\boldsymbol{k}) = \frac{\pm k_y - \mathrm{i}k_x}{\sqrt{2}k}\,,$$
$$C_{\mathrm{A}}^{v}(\boldsymbol{k}) = -\frac{1}{\sqrt{2}}\,, \quad C_{\mathrm{B}}^{v}(\boldsymbol{k}) = \frac{\pm k_y - \mathrm{i}k_x}{\sqrt{2}k}\,, \tag{9}$$

where $k = \sqrt{k_x^2 + k_y^2}$ is the distance from the K or K' point. Here the plus or minus sign for the k_y value is valid for the expansion around the K or K' point.

By expanding $\mathrm{e}^{\mathrm{i}\boldsymbol{k}\cdot\boldsymbol{b}_i}\boldsymbol{b}_i$ appearing in (7) around the K and K' points, we get the following result for the dipole vector up to linear terms in k_x and k_y for a given polarization vector $\boldsymbol{P} = \left(p_x, p_y, p_z\right)$,

$$\boldsymbol{D} = \left(d_x, d_y, d_z\right) = \pm\frac{3M}{2k}\left(-k_y, k_x, 0\right)\,. \tag{10}$$

Here the plus (minus) sign is for the K $\left(K'\right)$ point. Then the matrix element in (1) is proportional to

$$\boldsymbol{PD} = \pm\frac{3M}{2k}\left(p_y k_x - p_x k_y\right)\,. \tag{11}$$

This result shows that the line $p_y k_x - p_x k_y = 0$ in the 2D BZ becomes a node in the optical absorption for a given $\boldsymbol{P} = \left(p_x, p_y, p_z\right)$. For a given laser energy, the equi-energy line for optical absorption gives a circle (see Fig. 1b) around the K point with a wave vector $k = E_{\mathrm{laser}}/\sqrt{3}\gamma_0 a$, with $\gamma_0 = 2.89\,\mathrm{eV}$ [26, 27] for an optical experiment on carbon nanotubes. Thus we expect no optical absorption around the two crossing points of the line $p_y k_x - p_x k_y = 0$ with the circle.

In Fig. 2, we plot the absorption probability per unit time, which is the square of the matrix element in (2) in the 2D BZ of a graphene sheet for $E_{\mathrm{laser}} = 3\,\mathrm{eV}$ and (a) $\boldsymbol{P} = (0, 1)$, (b) $\boldsymbol{P} = (-1/2, \sqrt{3}/2)$, and (c) $\boldsymbol{P} = (1, 0)$. The dark region gives a large absorption coefficient. It is clear from the figure that nodes in the optical absorption appear on the vertical lines connecting the K and K' points in the 2D BZ $\left(k_x = 0, \pm 2\pi/\sqrt{3}a\right)$ in Fig. 2a. For different polarization directions in Fig. 2b and c, the nodes appear on the $p_y k_x - p_x k_y = 0$ lines around the K and K' points. Since we numerically solve the wavefunctions, the higher-order corrections for the node of (11) are included in Fig. 2. The existence of a node in the absorption coefficient as a function of $\boldsymbol{k}$ is a special effect that has never been observed in other materials.

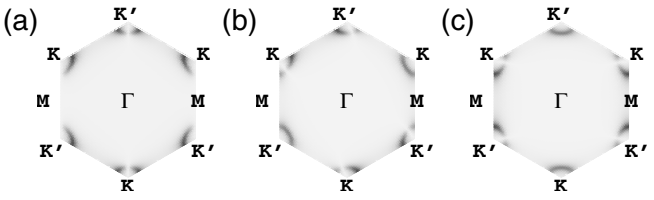

FIGURE 2 Plot of the optical absorption intensity (strong for dark area) as a function of k over the two-dimensional BZ of graphite. The polarization vectors are selected as **a** $\boldsymbol{P} = (0, 1)$, **b** $\boldsymbol{P} = (-1/2, \sqrt{3}/2)$, and **c** $\boldsymbol{P} = (1, 0)$. The laser energy is selected as $E_{\mathrm{laser}} = 3\,\mathrm{eV}$. It can be seen that the absorption is zero for certain wave-vector directions, and the condition for the vanishing absorption rotates with rotating $\boldsymbol{P}$ [12]

As far as the validity of the linear-k approximation for the energy and the wavefunction is concerned, the expression in (11) works well for specifying the node position. However, when the laser energy increases, the equi-energy contour is no longer a circle, but rather is changed into a triangle by the trigonal warping effect [28]. In this case, the higher-order corrections for (11) become important for describing the node positions [12].

It is difficult to see the node of $W(\boldsymbol{k})$ by photo-absorption experiments performed on graphene. However, when we consider nano-graphite ribbons [29], the wave vector in the direction perpendicular to the ribbon length becomes discrete, and thus we may be able to see the node by rotating the polarization of the light. Another possibility is to use angle-resolved photo-electron spectroscopy, if we consider the continuum states as the unoccupied states.

3 Optical absorption of single-wall carbon nanotubes

In the case of SWNTs, the dipole vector of the (n, m) SWNT is calculated by using the wavefunctions for the initial and final states that are specified by the subband index μ, $\mu = 1, \ldots, N$, and by the 1D wave vector k, $-\pi/T < k < \pi/T$ [2]. The energy subband index μ comes from the quantization of the wave vectors around the circumferential direction. N and T are the numbers of hexagons in the 1D unit cell and the 1D unit lattice vector, respectively. Hereafter we take the z axis to be the nanotube axis and the y axis to be on a B atom.

As is done in the case of 2D graphite, we decompose the wavefunction within the tight-binding scheme, and the dipole matrix element is thus decomposed into the sum of the atomic dipole vectors,

$$\boldsymbol{D} = \frac{\sqrt{3}M}{Na}\left[C_{\mathrm{A}}^{c*}(\boldsymbol{k})C_{\mathrm{B}}^{v}\left(\boldsymbol{k}'\right)\sum_{j}^{N}\mathrm{e}^{\mathrm{i}(\boldsymbol{k}-\boldsymbol{k}')\boldsymbol{R}_j^{\mathrm{B}}}U_z\left(\beta_j\right)\boldsymbol{v}_g - C_{\mathrm{B}}^{c*}(\boldsymbol{k})C_{\mathrm{A}}^{v}\left(\boldsymbol{k}'\right)\sum_{j}^{N}\mathrm{e}^{\mathrm{i}(\boldsymbol{k}-\boldsymbol{k}')\boldsymbol{R}_j^{\mathrm{A}}}U_z\left(\alpha_j\right)\boldsymbol{v}_g^{*}\right]\,. \tag{12}$$

Here $\boldsymbol{R}_j^{\mathrm{B}}$ and $\boldsymbol{R}_j^{\mathrm{A}}$ are the coordinates of the B and A carbon atoms in the SWNT unit cell. The vectors $\boldsymbol{k}'$ and $\boldsymbol{k}$ are the 2D initial and final wave vectors of the electron, respectively, and are given by

$$\boldsymbol{k} = \mu\boldsymbol{K}_1 + k\boldsymbol{K}_2\,, \tag{13}$$

where $\boldsymbol{K}_1$ and $\boldsymbol{K}_2$ are the reciprocal lattice vectors in the 2D BZ for a SWNT perpendicular and parallel to the nanotube-axis direction, respectively [2]. $\boldsymbol{v}_g$ is the atomic dipole vector of a SWNT for the B atom on the y axis, and $\boldsymbol{v}_g$ for each atom is obtained by rotating the atomic dipole vector of a carbon atom at the B atom for 2D graphite (1) around the y axis by $(-\pi/6 + \theta)$, where θ is the chiral angle, and then (2) rotating the dipole vectors around the nanotube axis U_z by angles α_j and β_j for the A and B atoms in the unit cell, respectively.

More explicitly, the angles are given by [2, 20]

$$\alpha_j = \frac{2\pi j}{N}\,, \quad \beta_j = \frac{2\pi j}{N} + \frac{2a}{d_t}\cos\left(\frac{\pi}{6} - \theta\right)\,, \tag{14}$$

where d_t is the diameter of a SWNT.

When we neglect the curvature effect of the cylindrical surface of the SWNT, the atomic dipole vector of the B atom is considered to be the same as that of 2D graphite. Thus we expect $\boldsymbol{D} = (d_x, 0, d_z)$, in which the y component of $\boldsymbol{D}$ becomes zero, since the direction perpendicular to the surface is y. For a carbon atom on a SWNT along the x axis, $\boldsymbol{D}$ becomes $\boldsymbol{D} = \left(0, d_y, d_z\right)$. The dipole selection rule for SWNTs is given by taking the sum of the atomic dipole vectors in (12) with the phase factor of $\mathrm{e}^{\mathrm{i}(\boldsymbol{k}-\boldsymbol{k}')\boldsymbol{R}_j^{\mathrm{A}}}$ or $\mathrm{e}^{\mathrm{i}(\boldsymbol{k}-\boldsymbol{k}')\boldsymbol{R}_j^{\mathrm{B}}}$.

In the case of the z polarization, $\boldsymbol{P} = (0, 0, p_z)$, the z component of the atomic dipole vectors, d_z, contributes to the absorption. Since d_z does not change direction by rotations around the z axis in the sum over j, the summation gives a non-zero value when $\boldsymbol{k} = \boldsymbol{k}'$. This gives the selection rule $\mu = \mu'$ for the energy subband index and $k = k'$ for the 1D wave number.

In the case of the x (or y) polarization, d_x (or d_y) contributes to the optical absorption. When we take the sum over j, d_x (or d_y) will rotate by 2π, which gives an additional phase $\left(\mathrm{e}^{2\pi\mathrm{i}/N}\right)^j$ to (12), which modifies the selection rule not for the 1D k vector, but only for the μ values. This is because the rotation of d_x (or d_y) does not correspond to movement along the z axis and thus there is no effect in 1D on[CE c] the k vectors. The effect on μ thus gives the selection rule $\mu - \mu' = \pm 1$ for x or y polarization [4, 12].

A further investigation [20] tells us that the dipole matrix element of a SWNT has the following general form for an axial chiral molecule,

$$\boldsymbol{D} = \left(\frac{D_+ + D_-}{2}, \pm\frac{D_+ - D_-}{2\mathrm{i}}, D_0\right)\,, \tag{15}$$

where D_+, D_-, and D_0 are functions of k given by (12), with the phase factors providing the dipole selection rules being $\mu - \mu' = +1, -1$, and 0, respectively. In (15), pm corresponds to left- and right-handed chiral nanotubes. Thus, for either the left- or the right-handed polarization of light propagating in the direction along the z axis, $\boldsymbol{P} = (p_x, \pm\mathrm{i}p_x, 0)$, the dipole selection rule is either $\mu - \mu' = +1$ or $\mu - \mu' = -1$ depending on the left- or right-handed chirality of the SWNTs [20]. These phenomena are generally observed in an axial chirality molecule and they are known as optical activity. However, because of the inversion symmetry in real space and because of time-reversal symmetry in k space, the optical spectra obtained for left- and right-handed polarizations may be the same [20]. Thus, in order to distinguish between right- and left-handed SWNTs, we need to break the symmetries by applying a magnetic field or lattice distortion. The detailed description of this phenomenon will be reported elsewhere.

4 Experiment

4.1 *Resonance Raman spectroscopy*

In resonance Raman spectroscopy, either the optical absorption or the optical emission enhances the Raman intensity in the incident or scattered resonance processes, respectively [13, 23, 24, 30–32].

As is discussed in the Introduction, the vHSs in the DOS for the 1D energy bands and in the corresponding JDOS are singular[CE d] and thus sharp vertical optical transitions in the 1D BZ are observed. Since the electronic structure of a SWNT consists of N energy subbands and each subband has a $1/\sqrt{E - E_i}$-type singularity at special k_i points for which the energy-dispersion relation becomes flat, the optical transition from a vHS for an occupied energy band to that for an unoccupied band gives significantly sharp spectral peaks, like those for a molecular level.

In the case of parallel polarization of light, the dipole selection rule gives us the transition from $-E_i$ in the bonding π energy band to E_i in the anti-bonding π^* energy band. The number of vHSs, however, is much smaller than the number of cutting lines, N, since most of the energy subbands are considered to be zone folded from a 2D graphite energy band [34]. The corresponding transition energies E_{ii} can be plotted for all (n, m) chiralities as a function of d_t [33] and the resulting plot is known as a Kataura plot, as shown in Fig. 3 [28]. Since the E_{ii} positions appear at different energies for a given diameter of SWNTs, we can easily distinguish a Raman signal for semiconducting SWNTs from that for metallic SWNTs [35, 36].

Because of the 1D lattice structure of SWNTs, the optical absorption for light polarized parallel to the nanotube axis is strong and the absorption for perpendicularly polarized light is strongly suppressed in an aligned SWNT bundle [33, 37–40] or an isolated SWNT [41–44]. The latter effect is understood by the so-called depolarization effect, in which the induced charge cancels the effect of the electric field of the

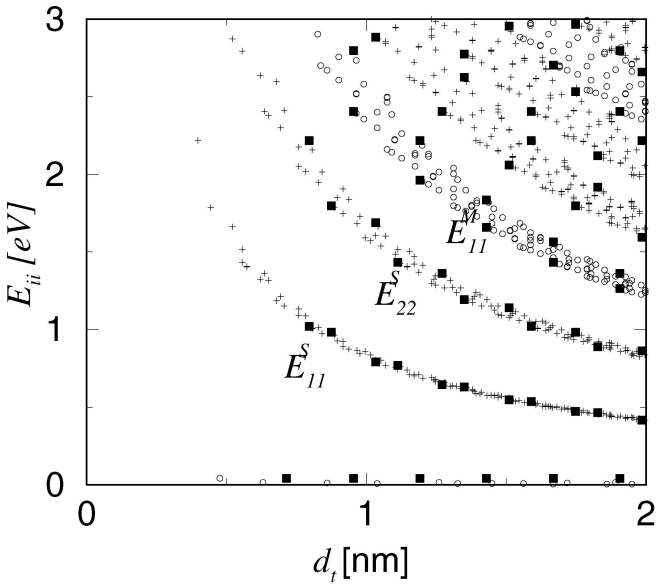

FIGURE 3 Calculation of the energy separations E_{ii} (d_t) for all (n, m) values as a function of nanotube diameter of 0.7 nm $< d_t <$ 3.0 nm (based on the work of Kataura et al. [33]). The results are based on the tight-binding model with transfer and overlap parameters $\gamma_0 = 2.9$ eV and $s = 0$ [2, 28]. The *crosses* and *open circles* denote the peaks of semiconducting and metallic nanotubes, respectively. *Filled squares* denote the E_{ii} (d_t) values for zigzag nanotubes, which determine the width of each E_{ii} (d_t) curve. Note the points for zero-gap metallic nanotubes along the abscissa

CE c Please check amended wording.
CE d Surely all vHSs are singular!

Editor's or typesetter's annotations (will be removed before the final TEX run)

nanotube [45–47]. This screening effect might not occur perfectly in the case of SWNT bundles, since the depolarization field from neighboring SWNTs smears out the screening to some extent. In fact, we do observe the perpendicular polarization spectra experimentally in non-aligned SWNT bundles [42–44, 48].

In some special experimental cases, the radial breathing modes (RBMs) (denoted by X in Fig. 4a) are observed in the middle of the energy-gap region between the E_{11}^S and E_{22}^S bands of the normal Kataura plot that is appropriate for parallel-polarized light. These special Raman signals do not appear in isolated single-wall nanotubes nor in well-aligned SWNT bundles. Further, we can not explain this signal by the Kataura plot for parallel polarization of light, even when we change the parameters for the electronic energy bands considerably. Thus we speculate that these spectral features come from the resonance Raman signal from perpendicularly polarized light [49]. In Fig. 4b we show a Kataura plot for perpendicularly polarized light and many of the observed RBM features can be fitted on this plot. The appearance of these RBM peaks is attributed to smearing out the depolarization effect in a sample of random orientation. A further investigation is needed to study this effect for such a sample.

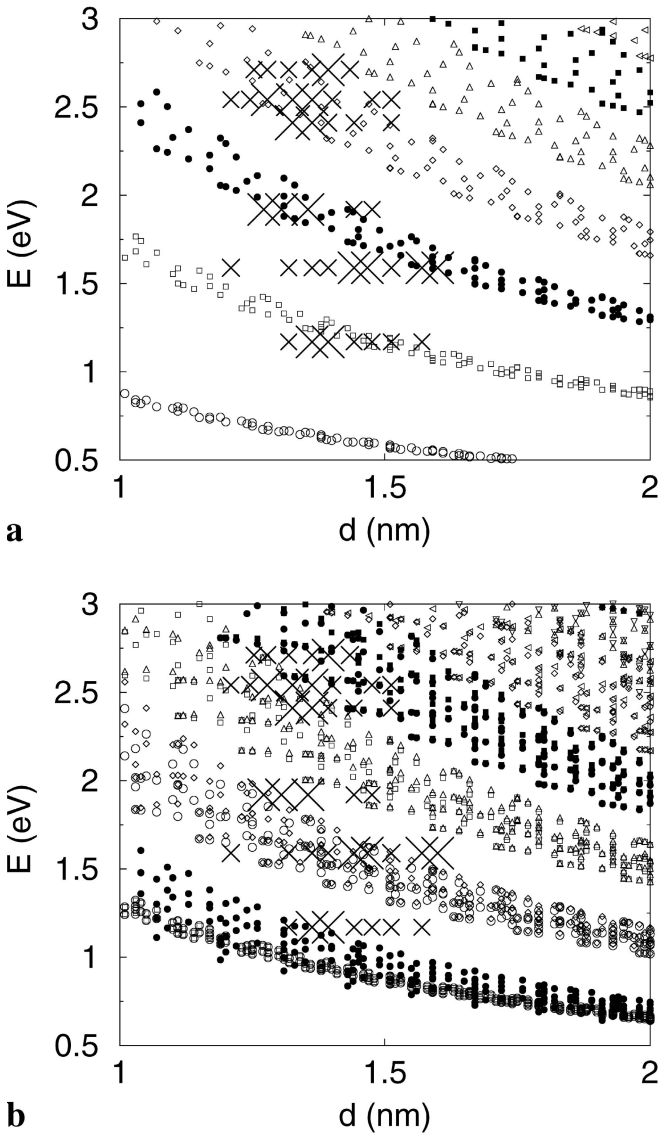

FIGURE 4 Calculation of the energy separations **a** E_{ii} (d_t) and **b** $E_{ii\pm1}$ (d_t) for all (n, m) values as a function of nanotube diameter of 0.7 nm $< d_t <$ 3.0 nm. The results are based on the tight-binding model with transfer and overlap parameters $\gamma_0 = 2.9$ eV and $s = 0$ [2, 28]. X denotes the experimental RBM signal whose size represents the relative intensity [49]

In our first paper on the (n, m) assignment for individual SWNTs using resonance Raman scattering [13], we adjusted the fitting parameters to explain all Raman signals of isolated SWNTs on a Si/SiO_2 surface. This fitting is valid for SWNTs with d_t around 1.4-nm diameter for SWNTs on Si/SiO_2 surfaces. This fitting works very well within an accuracy of 1 cm^{-1} for the RBM when combined with the optical absorption data [3]. For smaller-diameter nanotubes, the zone-folding scheme for the electronic structure does not work so well, and thus we expect some deviation of the experimental data from predictions of the tight-binding approximation for tube diameters below ~ 1 μm. Further, the effect of the substrate surface is also important. For some other Raman data from isolated SWNTs on a different surface or from SWNT bundles, the RBM frequencies are reported to be shifted by up to $\sim 10\,cm^{-1}$ [14]. Thus one needs to make some corrections when using the Kataura plot for different experimental conditions.

4.2 *Photo-luminescence*

Photo-luminescence (PL) from a SWNT has been reported for 0.4-nm SWNTs within a zeolite host [50] in an aqueous SDS suspension [15, 16, 22] and for suspended SWNTs in air [51]. A common situation for observing the photo-luminescence is that each SWNT is semiconducting and is well isolated. In the PL process, a photo-excited electron loses energy by recombining with a hole or by emitting phonons in a non-radiation process or by other optical processes, such as an Auger process, or plasmon generation. The existence of a nearby SWNT offers another possible electron-relaxation path for non-luminescence (NL) processes and these relaxation effects have been examined in fast optics studies in bundles [52, 53]. Especially, since a metallic SWNT has an energy dispersion which touches other dispersions at the Fermi level, NL recombination readily occurs for metallic SWNTs. In the case of semiconducting nanotubes, on the other hand, a photo-excited electron (or hole) loses energy and goes to the bottom of the conduction subband (or the top of the valence band) and then recombination between the electron and the hole occurs. Thus the radiation recombination resulting in a photo-luminescence signal for an isolated semiconducting SWNT can be observed.

The Raman process is a light-scattering process in which the scattered photon is observed. Thus, in the spectroscopic measurement of photons, we should be able to see both Raman and PL signals, in general. In fact, the coexistence of Raman and PL spectra has already been observed [21, 51], in which the Raman spectra give much sharper spectral features (1–10 cm^{-1}) than the PL spectral features ($\sim 100\,cm^{-1}$) in the case of SDS-suspended nanotubes in solution [21]. The corresponding lifetime of the PL process is about 100 fs, which is a reasonable value, based on fast optics experiments.

CE Please check section number.

Editor's or typesetter's annotations (will be removed before the final TEX run)

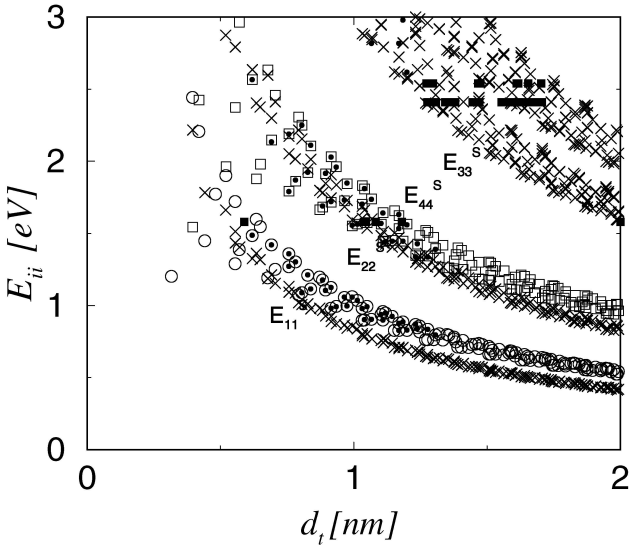

FIGURE 5 Kataura plot of a semiconducting nanotube. *Filled dots*, *open circle*, and *open square* denote, respectively, PL data and empirically fitted data for E_{11}^S and E_{22}^S [22]. *Filled square* denotes resonance Raman data [13, 23] only for the semiconducting nanotube. The *symbol* $\times$ shows a tight-binding result with $\gamma_0 = 2.9$ eV and $s = 0$ [2, 28]

In Fig. 5, we show the Kataura plot of semiconducting nanotubes taken from PL and resonance Raman spectra. Filled dots, open circles, and open squares denote, respectively, PL data and empirically fitted data for E_{11}^S and E_{22}^S transition energies [22]. Filled squares denote resonance Raman data [13, 23]. The symbol $\times$ shows the tight-binding results with $\gamma_0 = 2.9$ eV and $s = 0$ [2, 28]. In Fig. 5, we do not show the E_{11}^M plot for metallic SWNTs, since there is no PL data available for metallic nanotubes. As is discussed in Sect. 4.1 CE[e], the parameter of $\gamma_0 = 2.9$ eV is selected so as to reproduce the optical absorption data for 1.4-nm SWNTs. In fact the calculated E_{22}^S, E_{33}^S, and E_{44}^S points reproduce the PL data and Raman data rather well even for 1-nm SWNTs. Since there are no Raman measurements using E_{11}a^S, as far as we know, and since there are not many PL measurements for SWNTs with diameters larger than 1.4 nm, there is little common ground at present between the fitting procedures for the PL and Raman experiments.

However, E_{11}^S is clearly up-shifted relative to that of the PL shift. This PL shift is predicted to be due to a Coulomb interaction and is known as an exciton binding energy [54], which is observed in the PL spectra of SWNT bundles [55, 56]. According to Ando's results, the exciton levels appear at a higher energy position than would be expected from a simple tight binding energy gap model, without considering any Coulomb interaction due to the electron–electron interaction in 1D systems, and this effect is very large for the lowest-energy subbands in SWNTs [54, 57]. The corresponding energy for a single-electron excitation exists at a higher position than the exciton levels because the Coulomb interaction is repulsive, but there is no oscillator strength for the transition to this excitation because of the oscillator strength sum rule which is widely discussed in semiconductor physics [58]. This is our current understanding of the PL spectra. Further theoretical and experimental investigations are needed for understanding optical processes appearing in SWNTs.

5 Conclusion

In conclusion, we showed the optical absorption matrix elements of graphite and SWNTs as a function of $\boldsymbol{k}$. In 2D graphite, the absorption matrix elements show nodes on the equi-energy lines in the 2D BZ of graphite. In the case of SWNTs, we have a dipole selection rule for parallel- and perpendicularly polarized light. Raman spectroscopy shows a clear view of van Hove singular optical absorption not only for parallel-polarized light but also for perpendicularly polarized light for some SWNT bundles. Comparison of the Raman Kataura plot with the PL data gives a reasonable overlap with each other and with the calculated transition energies. However, we need a more sophisticated model for explaining the wide range of diameters and transition energies in these spectra.

ACKNOWLEDGEMENTS R.S. acknowledges Prof. R. Bruce Weisman for providing experimental Kataura plot data and Mr. Zilong Chen for preparing Fig. 5. The authors acknowledge many experimental collaborators for providing important Raman spectra of SWNTs. R.S. acknowledges a Grant-in-Aid (No. 13 440 091) from the Ministry of Education, Japan. The MIT authors acknowledge support under NSF Grant Nos. DMR 01-16042 and INT 00-00408. A.J. and M.A.P. acknowledge support by the Instituto de Nanociências, Brazil. A.G.S.F. acknowledges financial support from CAPES-Brazil under a PRODOC-22001018 grant.

REFERENCES

1 M.S. Dresselhaus, G. Dresselhaus, P.C. Eklund: *Science of Fullerenes and Carbon Nanotubes* (Academic, New York, NY, San Diego, CA 1996)
2 R. Saito, G. Dresselhaus, M.S. Dresselhaus: *Physical Properties of Carbon Nanotubes* (Imperial College Press, London 1998)
3 R. Saito, H. Kataura: in *Carbon Nanotubes: Synthesis, Structure, Properties and Applications*, ed. by M.S. Dresselhaus, G. Dresselhaus, Ph. Avouris (Springer Ser. Top. Appl. Phys. **80**) (Springer, Berlin 2001)
4 H. Ajiki, T. Ando: Physica B: Condens. Matter **201**, 349 (1994)
5 H. Ajiki, T. Ando: Jpn. J. Appl. Phys. Suppl. **34**, 107 (1995)
6 R. Saito, M. Fujita, G. Dresselhaus, M.S. Dresselhaus: Phys. Rev. B **46**, 1804 (1992)
7 R. Saito, M. Fujita, G. Dresselhaus, M.S. Dresselhaus: Appl. Phys. Lett. **60**, 2204 (1992)
8 T. Ando, T. Nakanishi, R. Saito: J. Phys. Soc. Jpn. **67**, 2857 (1998)
9 C. Thomsen, S. Reich: Phys. Rev. Lett. **85**, 5214 (2000)
10 R. Saito, A. Jorio, A.G. Souza Filho, G. Dresselhaus, M.S. Dresselhaus, M.A. Pimenta: Phys. Rev. Lett. **88**, 027 401 (2002)
11 J. Kürti, V. Zólyomi, A. Grüneis, H. Kuzmany: Phys. Rev. B **65**, 165 433 (2002)
12 A. Grüneis, R. Saito, G.G. Samsonidze, T. Kimura, M.A. Pimenta, A. Jorio, A.G. Souza Filho, G. Dresselhaus, M.S. Dresselhaus: Phys. Rev. B **67**, 165 402 (2003)
13 A. Jorio, R. Saito, J.H. Hafner, C.M. Lieber, M. Hunter, T. McClure, G. Dresselhaus, M.S. Dresselhaus: Phys. Rev. Lett. **86**, 1118 (2001)
14 X. Zhao, Y. Ando, L.-C. Qin, H. Kataura, Y. Maniwa, R. Saito: Appl. Phys. Lett. **81**, 2550 (2002)
15 M.J. O'Connell, S.M. Bachilo, X.B. Huffman, V.C. Moore, M.S. Strano, E.H. Haroz, K.L. Rialon, P.J. Boul, W.H. Noon, C. Kittrell, J. Ma, R.H. Hauge, R.B. Weisman, R.E. Smalley: Science **297**, 593 (2002)
16 S.M. Bachilo, M.S. Strano, C. Kittrell, R.H. Hauge, R.E. Smalley, R.B. Weisman: Science **298**, 2361 (2002)
17 K. Kneipp, H. Kneipp, P. Corio, S.D.M. Brown, K. Shafer, J. Motz, L.T. Perelman, E.B. Hanlon, A. Marucci, G. Dresselhaus, M.S. Dresselhaus: Phys. Rev. Lett. **84**, 3470 (2000)
18 A. Jorio, A.G. Souza Filho, G. Dresselhaus, M.S. Dresselhaus, R. Saito, J.H. Hafner, C.M. Lieber, F.M. Matinaga, M.S.S. Dantas, M.A. Pimenta: Phys. Rev. B **63**, 245 416 (2001)
19 A. Jorio, M.A. Pimenta, A.G. Souza Filho, G.G. Samsonidze, A.K. Swan, M.S. Ünlü, B.B. Goldberg, R. Saito, G. Dresselhaus, M.S. Dresselhaus: Phys. Rev. Lett. **90**, 107 403 (2003)

CE[f] Please update this reference.

Editor's or typesetter's annotations (will be removed before the final TEX run)

20 G.G. Samsonidze, A. Grüneis, R. Saito, A. Jorio, M.A. Pimenta, A.G. Souza Filho, G. Dresselhaus, M.S. Dresselhaus: unpublished
21 M.S. Strano, M.K. Miller, M.J. Allen, V.C. Moore, M.J. O'Connell, C. Kittrell, R.H. Hauge, R.E. Smalley: J. Nanosci. Nanotechnol., in press (2003) CE[f]
22 R.B. Weisman, S.M. Bachilo: Nano Lett. **3**, 1235 (2003)
23 M.S. Dresselhaus, G. Dresselhaus, A. Jorio, A.G. Souza Filho, G.G. Samsonidze, R. Saito: J. Nanosci. Nanotechnol. **3**, 19 (2003)
24 A.G. Souza Filho, A. Jorio, G.G. Samsonidze, G. Dresselhaus, R. Saito, M.S. Dresselhaus: Nanotechnology **14**, 1130 (2003)
25 P.L. McEuen, M. Bockrath, D.H. Cobden, Y.G. Yoon, S.G. Louie: Phys. Rev. Lett. **83**, 5098 (1999)
26 A.G. Souza Filho, A. Jorio, J.H. Hafner, C.M. Lieber, R. Saito, M.A. Pimenta, G. Dresselhaus, M.S. Dresselhaus: Phys. Rev. B **63**, 241 404R (2001)
27 Z. Yu, L.E. Brus: J. Phys. Chem. B **105**, 743 (2001)
28 R. Saito, G. Dresselhaus, M.S. Dresselhaus: Phys. Rev. B **61**, 2981 (2000)
29 K. Wakabayashi, M. Fujita, H. Ajiki, M. Sigrist: Phys. Rev. B **59**, 8271 (1999)
30 A.M. Rao, E. Richter, S. Bandow, B. Chase, P.C. Eklund, K.W. Williams, S. Fang, K.R. Subbaswamy, M. Menon, A. Thess, R.E. Smalley, G. Dresselhaus, M.S. Dresselhaus: Science **275**, 187 (1997)
31 M.S. Dresselhaus, P.C. Eklund: Adv. Phys. **49**, 705 (2000)
32 R. Saito, A. Grüneis, G.G. Samsonidze, V.W. Brar, G. Dresselhaus, M.S. Dresselhaus, A. Jorio, L.G. Cançado, C. Fantini, M.A. Pimenta, A.G. Souza Filho: unpublished
33 H. Kataura, Y. Kumazawa, N. Kojima, Y. Maniwa, I. Umezu, S. Masubuchi, S. Kazama, X. Zhao, Y. Ando, Y. Ohtsuka, S. Suzuki, Y. Achiba: in *Proc. Int. Winter Sch. Electronic Properties of Novel Materials (IWEP-NM'99)*, ed. by H. Kuzmany, M. Mehring, J. Fink (American Institute of Physics, Woodbury, NY 1999) [AIP Conf. Proc. **486**, 328 (1999)]
34 G.G. Samsonidze, R. Saito, A. Jorio, M.A. Pimenta, A.G. Souza Filho, A. Grüneis, G. Dresselhaus, M.S. Dresselhaus: J. Nanosci. Nanotechnol., unpublished CE[g]
35 M.A. Pimenta, A. Marucci, S.D.M. Brown, M.J. Matthews, A.M. Rao, P.C. Eklund, R.E. Smalley, G. Dresselhaus, M.S. Dresselhaus: J. Mater. Res. **13**, 2396 (1998)
36 M.A. Pimenta, A. Marucci, S. Empedocles, M. Bawendi, E.B. Hanlon, A.M. Rao, P.C. Eklund, R.E. Smalley, G. Dresselhaus, M.S. Dresselhaus: Phys. Rev. B Rapid **58**, R16 016 (1998)
37 S. Kazaoui, N. Minami, R. Jacquemin, H. Kataura, Y. Achiba: Phys. Rev. B **60**, 13 339 (1999)
38 J. Hwang, H.H. Gommans, A. Ugawa, H. Tashiro, R. Haggenmueller, K.I. Winey, J.E. Fischer, D.B. Tanner, A.G. Rinzler: Phys. Rev. B **62**, R13 310 (2000)
39 M.F. Lin: Phys. Rev. B **62**, 13 153 (2000)
40 F.J. Garcia-Vidal, J.M. Pitarke: Eur. Phys. J. B **22**, 257 (2001)
41 G.S. Duesberg, I. Loa, M. Burghard, K. Syassen, S. Roth: Phys. Rev. Lett. **85**, 5436 (2000)
42 Z. Yu, L.E. Brus: J. Phys. Chem. B **105**, 1123 (2001)
43 A. Jorio, G. Dresselhaus, M.S. Dresselhaus, M. Souza, M.S.S. Dantas, M.A. Pimenta, A.M. Rao, R. Saito, C. Liu, H.M. Cheng: Phys. Rev. Lett. **85**, 2617 (2000)
44 A. Jorio, A.G. Souza Filho, V.W. Brar, A.K. Swan, M.S. Ünlü, B.B. Goldberg, A. Righi, J.H. Hafner, C.M. Lieber, R. Saito, G. Dresselhaus, M.S. Dresselhaus: Phys. Rev. B Rapid **65**, R121 402 (2002)
45 H. Ajiki, T. Ando: Physica **201**, 349 (1994); T. Ando: J. Phys. Soc. Jpn. **66**, 1066 (1997)
46 L.X. Benedict, S.G. Louie, M.L. Cohen: Phys. Rev. B **52**, 8541 (1995)
47 A.G. Marinopoulos, L. Reining, A. Rubio, N. Vast: Phys. Rev. Lett. **91**, 046 402 (2003) and references therein
48 A.M. Rao, A. Jorio, M.A. Pimenta, M.S.S. Dantas, R. Saito, G. Dresselhaus, M.S. Dresselhaus: Phys. Rev. Lett. **84**, 1820 (2000); see also: Comment in Phys. Rev. Lett. **85**, 3545 (2000)
49 A. Grueneis et al. CE[h]: unpublished
50 Z.M. Li, Z.K. Tang, H.J. Liu, N. Wang, C.T. Chan, R. Saito, S. Okada, G.D. Li, J.S. Chen, N. Nagasawa, S. Tsuda: Phys. Rev. Lett. **87**, 127 401 (2001)
51 J. Lefebvre, Y. Homma, P. Finnie: Phys. Rev. Lett. **90**, 217 401 (2003)
52 T. Hertel, E. Knoesel, M. Wolf, G. Ertl: Phys. Rev. Lett. **76**, 535 (1996)
53 G. Moos, R. Fasel, T. Hertel: J. Nanosci. Nanotechnol. **3**, 145 (2003)
54 T. Ando: J. Phys. Soc. Jpn. **66**, 1066 (1997)
55 M. Ichida, S. Mizuno, Y. Tani, Y. Saito, A. Nakamura: J. Phys. Soc. Jpn. **68**, 3131 (1999)
56 M. Ichida, S. Mizuno, S. Kuno, Y. Saito, H. Kataura, Y. Achiba, A. Nakamura: in *Proc. 25th Int. Conf. Physics of Semiconductors, Osaka, Japan*, ed. by N. Miura, T. Ando (Japanese Physical Society, Tokyo 2000) p. 1685
57 C.L. Kane, E.J. Mele: Phys. Rev. Lett. **90**, 207 401 (2003)
58 S.G. Louie: NT03 presentation, Seoul, Korea (2003) CE[i]

CE[g] Please update this reference.
CE[h] Please give names of all the authors.
CE[i] Please clarify 'NT03'.

Editor's or typesetter's annotations (will be removed before the final TEX run)